8th International Conference on Power Electronics - ECCE Asia
May 30-June 3, 2011, The Shilla Jeju, Korea

A Full Study of a PHEV Charging Facility based on Global Optimization and Real-Time Simulation

Ernesto Inoa, Feng Guo, and Jin Wang
The Ohio State University, Columbus, Ohio, USA

Woongchul Choi
Kookmin University, Seoul, Korea

Abstract-- **This paper provides insight into two important issues arising in scenarios with high level of penetration of photovoltaic (PVs) based Plug-In Hybrid Vehicles (PHEVs) charging stations. Namely, the paper proposes a method to determine the optimal size of the local energy storage (LES) for a charging facility and also develops the control strategy for the proper integration of these LES and PVs with the PHEV charging stations. The proposed LES sizing method, which is based on optimal control theory, minimizes a cost function based on the average value of kWh price, irradiance and PHEVs usage patterns. A power-loss/temperature model and a temperature based charging strategy, previously developed by the authors, are utilized in determine the optimized LES sizing. Then, with the optimized facility parameters, a detailed circuit model of a charging facility is built. Control strategies of the power electronics networks in this charging facility is proposed and tested with real time simulations.**

Index Terms— **Optimization, PHEV Charging, Real-Time Simulation.**

I. INTRODUCTION

The number of Plug-in Hybrid Electric Vehicles (PHEV's) is expected to increase rapidly in the coming years [1]. It is an urgent task to study the design and control of charging facilities for PHEVs. This paper presents a full study of a hypothetical charging facility for delivery trucks. It is assumed that the facility takes power from both electrical power grid and photovoltaic (PV) shades. A Lithium-Ion battery pack is also installed in this facility as a local energy storage system to lower the overall cost of installation and operation.

While the size of the total size of the PV shades could be decided by the size of the roof or the shades of the vehicles, to determine the size of the Local Energy Storage System (LES) is quite challenging. Several recent papers [2]-[6] and IEE standards/guidelines [7]-[8] have been published to address many different aspects of battery sizing for PV installations. Nevertheless, no study has been reported with specific PHEV related load profiles, which include vehicle charging strategies and usage patterns. Most published papers deal with very specific scenarios in which lead-acid batteries are used. For instance, [9] studies the effect of different battery-bank sizes on the performance of a PV system whereas [10] studies the effect of size on the lifetime of the battery itself; [11] optimizes the battery size based on the probability of surviving an outage while maximizing savings due to demand shift; and [12] optimizes with respect to the environmental impact of the battery size.

Besides battery size, control strategy of the multiple power electronics circuits in the charging facility also presents as a great challenge, especially in the case of dynamic islanding, where the local energy storage and PV panels are solely responsible for supplying power to the loads [13]. In [14], Huang et. al. describe the different control strategies in grid-connected mode and islanding mode. It is also commonly accepted that during grid-connected mode, current-based control should be used for the inverters whereas, during islanding mode, a voltage-based control should be used. Several authors [15]] – [[16] propose different control method to guarantee the seamless transfer from grid-connected mode to islanding mode.

This paper first develops a battery sizing algorithm that minimizes the cost of energy consumed by the charging facility. To model the load, a battery model based on the power-loss and temperature change incurs in the battery during the charging process [17] is utilized. Due to the use of this battery power-loss/temperature model, a charging current profile that maximizes the performance of a PHEV battery in cold weather can be determined. This optimized charging profile is in general different from the ubiquitous Constant Current/Current Constant Voltage (CC/CV).

With optimized sizing of local energy storage devices, a detailed circuit model of the charging facility is developed. A comprehensive control strategy is proposed to coordinate the grid tied inverters and converters in the system during both grid-connected mode and islanding mode. Special consideration is also given to guarantee the seamless transfer from grid-connected mode to islanding mode. While experimental setup for this kind of complex and high cost system is not feasible, real-time simulation were carried out to prove the effectiveness of the proposed control strategies.

This paper is divided into four sections. The next section presents the battery sizing algorithm while Section III shows the proposed control strategy and real-time simulation results. Section IV concludes the paper and makes final remarks.

978-1-61284-957-7/11/$26.00 ©2011 IEEE

II. BATTERY SIZING ALGORITHM

A. Algorithm Overview

The proposed battery sizing algorithm is developed in the context of a distribution center in which PHEV distribution trucks are docked and several PV panels are installed. Essentially, the proposed algorithm is based on the minimization of the cost function defined in equation (1), in which the cost of the energy consumed is calculated. Equation (1) has three terms; the first two are the daily prorated cost of buying, installing and maintaining the LES and the PV system, respectively. The last term reflects the cost of energy paid to the grid, that is, the energy consumed by the load minus the energy supplied by the LES and the PV system (or any other source installed in the facility).

Intuitively, the first term tends to increase in a relatively linear fashion as the size of the LES increases. The last term of (1) tends to decrease in an exponential fashion as the size of the LES increases. Therefore, a minimum for (1) could be found when the size of the LES is varied.

$$\begin{aligned}\text{DailyCost} \;=\; & \text{PriceBattPack}|_{day} + \text{PricePVSystem}|_{day} \\ & + \int_{day} \left(P_{Load}(t) - P_{PV}(t) - P_{LES}(t)\right)\cdot \text{kWhPr}(t)\; dt\end{aligned} \tag{1}$$

By translating the different source/load profiles and subsystem sizes into their resultant monetary cost, the battery sizing algorithm can be applied to an unlimited number of source/load configurations.

The algorithm contains the following steps:

1) After the profile of the load, kWh price, and irradiation profile are found, pick a small size for the LES as a starting point.

2) Apply an optimization tool (GPOPS [18]-[21]) to minimize equation (1), which results in a minimized daily cost for the picked battery size. Basically, GPOPS will minimize the integral term in Eq. (1) by determining an optimal charging/discharging profile for the LES, i.e., when the electricity price is high, the LES will send power to the grid, whereas when the electricity price is low, the LES will absorb power from the grid.

3) Change the battery size linearly and repeat step (2) to form a curve that shows the relationship between daily cost and the sizing of the LES. An optimized LES size will be identified as the minimum in this curve.

B. Load Profile

In order to apply the described algorithm, the profiles of load, kWh price, and irradiation are needed. Since irradiation profile could be decided based on historical data, only the load profile is described.

Two groups of distribution trucks (PHEVs) are assumed. According to the results obtained in [17], in cold weather the performance of a PHEV's battery increases if most of the charge is applied at the end of the charging process, whereas in hot weather CC/CV is near optimal in terms of charging efficiency [22]. The load profile could be calculated with the charging profiles and the Li-Ion battery model as shown in Fig. 1.

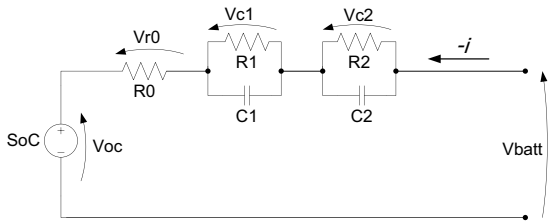

Fig. 1. Battery-Cell Equivalent Circuit.

Based on this model, dynamic equations are obtained by considering the current as the control input, and choosing the state-variables to be

$$\vec{x} = \begin{bmatrix} SoC & v_{c1} & v_{c2} & \Delta T \end{bmatrix}^T, \tag{2}$$

where SoC is State of Charge of the battery, ΔT is the temperature difference between the hottest point in the battery and the ambient temperature, and v_{c1} and v_{c2} are the capacitor voltages. Therefore, the dynamic equations of the battery, in state-state form, becomes

$$\begin{aligned}
\dot{x}_1 &= \frac{-1}{3600\cdot C(x_4 + T_{amb})}u \\
\dot{x}_2 &= \frac{-1}{R_1(x_1, x_4 + T_{amb})\cdot C_1(x_1, x_4 + T_{amb})}\vec{x}_2 + \frac{1}{C_1(x_1, x_4 + T_{amb})}u \\
\dot{x}_3 &= \frac{-1}{R_2(x_1, x_4 + T_{amb})\cdot C_2(x_1, x_4 + T_{amb})}\vec{x}_3 + \frac{1}{C_2(x_1, x_4 + T_{amb})}u \\
\dot{x}_4 &= \frac{-1}{R_{temperature}\cdot C_{temperature}}\vec{x}_4 + \frac{1}{C_{temperature}}P_{loss}
\end{aligned},$$

where $C(x_4 + T_{amp})$ is the battery's capacity and T_{amb} is the ambient temperature. $R_{temperature}$ and $C_{temperature}$ account for the battery's thermal model; P_{loss} is the power loss in the resistive components of the battery model, which is determined by the charging profile. As indicated in the previous discussion, optimal charging profiles and the battery model are used in the battery sizing algorithm.

C. Calculation Results

Several assumptions, in terms of cost and power ratings of the PV panels, were made in order to run the battery sizing algorithm. Fundamentally, the charger of the LES is Level II. The facility has a PV system of 15 kWp. Finally, cost estimates for Li-Ion batteries, provided by the US Department of Energy [23], of US$300/kW and US$500/kW were used in the calculation.

Results for different cases are plotted in Fig. 2 to Fig. 4. Fig. 2 and 3 show the results for the load profiles used in cold weather, with and without a PV system installed. The minima are at the same values of LES size, since the amount of received solar energy is not high enough to validate make a major impact of the daily operation cost.

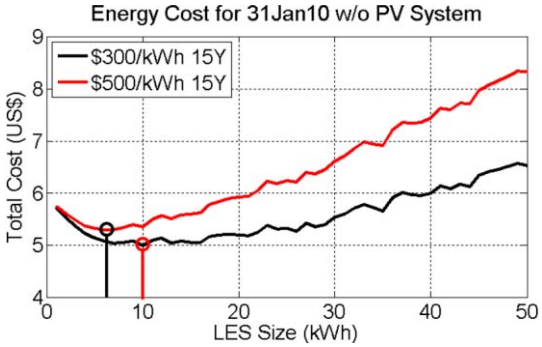

Fig. 2. Daily cost, during winter w/o PV.

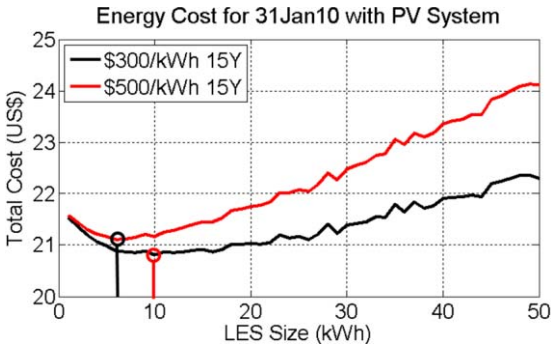

Fig. 3. Daily cost, during winter with PV.

The comparison between Figure 2 and 3 shows that the installation cost of the PV systems has major impact on the overall daily cost of the system.

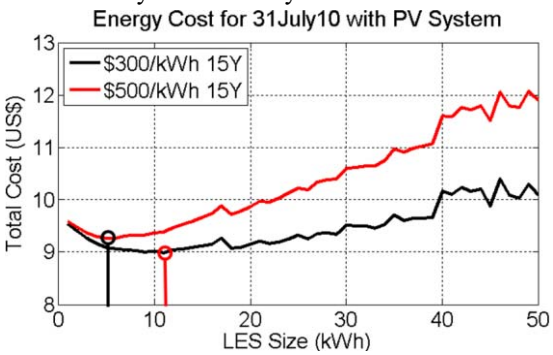

Fig. 4. Daily cost, during summer with PV.

Fig. 4 shows the result for a similar system in hot weather, where a different load profile is used. Also, since it is during the middle of the boreal summer season, there is an increase in the intensity and length of irradiation obtained. Therefore, it makes economic sense to have a bigger LES to save the extra solar energy so that it can be used when the load demands it. As a consequence, the minimum happens at the LES size of 11kWh instead of 10 kWh for the instance when the cost estimate is of US$300/kWh.

III. Real-Time Simulation of Charging Station

A. System Description

To integrate the LES and PV into PHEV charging station and realize the operation criterion discussed in Section II, a system-level PHEV charging station model is built with advanced real time simulation system. The system schematic and detailed circuit topology for each branch are shown in Fig. 5.

The charging station is able to work in two modes: grid-connected mode and islanding mode. During grid-connected mode, the circuit breaker is closed. The operation of the LES follows the criterion listed in Section II, which is, when the electricity price is high, the LES will send power to PHEV batteries; while when the electricity price is low, the LES will absorb power from the grid. Once a failure happens on the grid side, the circuit breaker will open, and the charging station will operate in islanding mode. Under this condition, the LES and PV will provide power to charge PHEV batteries. No matter in which mode, the PV will always be controlled to output maximum power to the charging station.

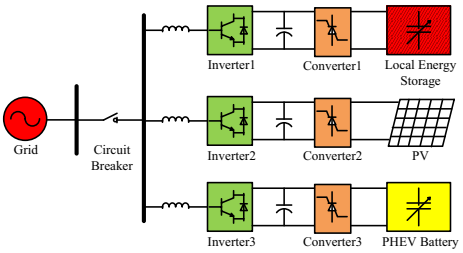

(a) System schematic

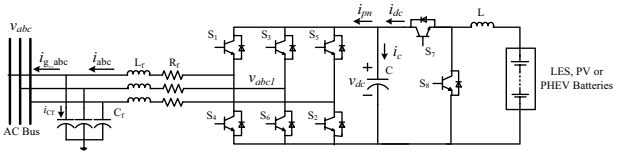

(b) Circuit topology for each branch

Fig. 5. System schematic and the detailed circuit topology.

According to Fig. 5(b), the equation to describe the voltage and current relation on ac side can be expressed as

$$v_{abc} = R_f i_{abc} + L_f \frac{d}{dt} i_{abc} + v_{abc1}, \tag{3}$$

where R_f and L_f are the line resistor and inductor, respectively. Using the transformation matrix in (4), where "f" represents any electrical parameter, (3) can be transformed into a d-q rotating reference frame. After transformation, equations are given in (3).

$$\begin{bmatrix} f_d \\ f_q \\ f_0 \end{bmatrix} = \frac{2}{3} \begin{bmatrix} \cos(\omega t) & \cos(\omega t - 2\pi/3) & \cos(\omega t + 2\pi/3) \\ -\sin(\omega t) & -\sin(\omega t - 2\pi/3) & -\sin(\omega t + 2\pi/3) \\ 0.5 & 0.5 & 0.5 \end{bmatrix} \begin{bmatrix} f_a \\ f_b \\ f_c \end{bmatrix} \tag{4}$$

$$\begin{aligned} v_d &= R_f i_d + L_f \frac{di_d}{dt} - \omega L_f i_q + v_{d1} \\ v_q &= R_f i_q + L_f \frac{di_q}{dt} + \omega L_f i_d + v_{q1} \end{aligned}, \tag{5}$$

Meanwhile, in d-q rotating reference frame, the active and reactive power can be expressed as

$$\begin{aligned} P &= \frac{3}{2}(v_d i_d + v_q i_q) \\ Q &= \frac{3}{2}(v_d i_q + v_q i_d) \end{aligned}. \tag{6}$$

To simplify the analysis, the rotating d-axis is synchronized with the supply voltage vector, which makes v_q=0. Neglecting harmonics and losses in the circuit, the relationship between ac side and dc side can

be found as

$$v_{dc} i_{dc} = \frac{3}{2} v_d i_d . \quad (7)$$

B. Control Strategy

The aim of the controller design is to make sure the system works properly in both grid-connected mode and islanding mode. Meanwhile, the LES, PV and PHEV batteries should be controlled to operation under the criterion discussed in Section II. More importantly, the controller should avoid large voltage and current spike during the transition from grid-connected mode to islanding mode.

1) *Grid-connected Mode*

For the grid connected mode, a multi-loop controller is used for all the three utility interactive inverters, as is shown in Fig. 6 (a). The control objective of the inverters is to keep the DC-link voltage constant regardless of the power change in their connected units. Therefore, the outer loop of the controller is a voltage loop with DC-link voltage as feedback. The inner loop is a grid current loop, with the active current reference generated by the outer voltage loop and reactive current reference set to 0. Based on equations (5), (6) and (7), the simplified dc bus output-voltage-to-reference-voltage control diagram is shown in Fig. 6(b).

In order to design a system with fast dynamic response and small steady state error between DC-link voltage and its reference value, the inner current loop controller and outer voltage loop controller should be considered separately [24].

The inner current loop should have a much faster response time than the outer voltage loop. Therefore, on one hand, the bandwidth should be designed as high as

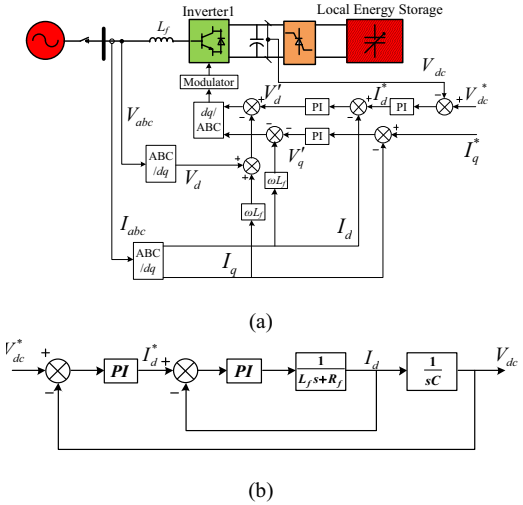

(a)

(b)

Fig. 6. Inverter controller in grid-connected mode.

possible. On the other hand, the bandwidth should be designed to remove the switching harmonics, so it should be no more than half of the switching frequency. A compromise value should be decided based on these two criteria [25]. A Proportional-Integral (PI) controller is utilized here to achieve a good control performance. The closed current loop transfer function is shown in (8).

$$\frac{I_d}{I_d^*} = \frac{K_{cp} s + K_{ci}}{L_f s^2 + (K_{cp} + R_f) s + K_{ci}}, \quad (8)$$

where K_{cp} and K_{ci} are the proportional and integral gain of the current loop PI controller, respectively.

After designing the current control loop, the closed voltage loop transfer function with a PI controller can be expressed as

$$\begin{aligned} &\frac{V_{dc}}{V_{dc}^*} = \frac{M(s)}{N(s)} \\ &M(s) = K_{cp} K_{vp} s^2 + (K_{cp} K_{vi} + K_{ci} K_{vp}) s + K_{vi} K_{ci}, \\ &N(s) = L_f C s^4 + (C K_{cp} + R_f C) s^3 + (K_{cp} K_{vp} + K_{ci} C) s^2 \\ &\quad + (K_{cp} K_{vi} + K_{ci} K_{vp}) s + K_{vi} K_{ci} \end{aligned} \quad (9)$$

where C is the dc bus capacitor, K_{vp} and K_{vi} are the proportional and integral gain of the voltage loop PI controller, respectively.

Considering three converters, the LES connected converter and PHEV batteries connected converter are working in current control mode. Their current commands are determined by the criterion described in Section II. While the PV connected converter is working with Maximum Power Point Tracking (MPPT) strategy.

2) *Islanding Mode*

For the islanding mode, the inverters and converters that are connected to PV and PHEV batteries still keep the same control strategy as in the grid-connected mode. While for the LES connected inverter, the same multi-loop control structure is used, but with the ac bus voltage as the feedback in the outer voltage loop, as is shown in Fig. 7(a). This is because in the islanding mode, the control objective of this inverter is to keep the ac bus voltage constant. The inner loop is the same current loop as in the grid-connected mode [26]. Because of the similarity between grid-connected mode controller and islanding mode controller, a seamless transfer from grid-connected mode to islanding mode can be achieved by this design. The simplified ac bus output-voltage-to-reference-voltage control diagram is shown in Fig. 7(b).

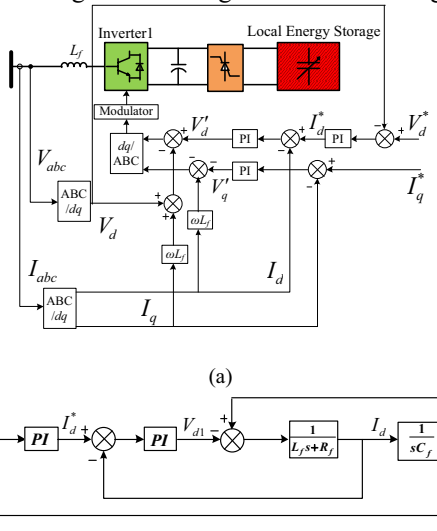

(a)

(b)

Fig. 7. The controller of LES-connected inverter in islanding mode.

The design process of the multi-loop controller is the same as that in grid-connected model. The inner current loop controller will keep unchanged, and the closed loop transfer function is shown in (10).

$$\frac{I_d}{I_d^*} = \frac{K_{cp}C_f s + K_{ci}C_f}{L_f C_f s^2 + (K_{cp}C_f + R_f C_f)s + (K_{ci}C_f + 1)}, \quad (10)$$

where C_f is the line capacitor.

The outer voltage loop should have a slower response time than the current loop. The closed loop transfer function from the reference ac voltage to the output ac voltage is shown in (11).

$$\frac{V_d}{V_d^*} = \frac{P(s)}{Q(s)}$$
$$P(s) = K_{cp}K'_{vp}s^2 + (K_{cp}K'_{vi} + K_{ci}K'_{vp})s + K'_{vi}K_{ci}, \quad (11)$$
$$Q(s) = L_f C_f s^4 + (K_{cp}C_f + R_f C_f)s^3$$
$$+ (1 + K_{cp}K'_{vp} + K_{ci}C_f)s^2 + (K_{cp}K'_{vi} + K_{ci}K'_{vp})s + K'_{vi}K_{ci}$$

where K'_{vp} and K'_{vi} are the proportional and integral gain of the voltage loop PI controller, respectively.

As mentioned above, in the islanding mode, the LES connected inverter is used to control the ac bus voltage. Therefore, the control purpose of the LES connected converter is changed to control the DC-link voltage. Considering that the output current of the LES should also be restrictedly controlled, a multi-loop controller with outer voltage loop and inner current loop is designed for this converter. The outer voltage control loop uses DC-link voltage as feedback, which will generate a reference value for the inner current control loop.

C. Simulation Results

Real time simulation is carried out for the case where the system transfers from grid-connected mode to islanding mode. In the simulation, it is assumed that at certain time, a three phase short circuit happens on the grid side. The protection unit detects this failure and opens the main circuit breaker. To simplify the simulation, assume that in the grid-connected mode, right before the circuit breaker opens, the LES is sending constant 7 kW power to the system, and during the islanding mode, the LES and PV can provide enough power to charge PHEV batteries.

The simulation parameters are listed in Table I, which is based on the optimized parameters from Section II. The real time simulation results of the internal dc bus voltage, the ac side line-line voltage, ac currents from LES inverter, currents from the power grid, and PHEV charging currents are shown in Figure 8.

TABLE I
SIMULATION PARAMETERS

System Frequency f	60 Hz
Switching Frequency f_{sw}	10 kHz
Dc Bus Voltage V_{dc}	800 V
Capacitor C	2.2 mF
Ac Bus Voltage V_{bus}	240 $V_{L\text{-}g}$
Inductor L_f	0.76 mH
Resistor R_f	1 mΩ
Capacitor C_f	8.3 μF
PV Power Output P_{pv}	3 kW
PHEV Power Consumption P_{phev}	12 kW

The result illustrates that the system operates correctly in both grid-connected mode and islanding mode. Furthermore, the voltage and current spike during the transition from grid-connected mode to islanding mode are within three times of their normal values, which are not significant. Therefore, the proposed control strategy is effectively. Combined with the discussion in Section II, it also provides a globally economic approach to operate LES and PV in the PHEV charging station.

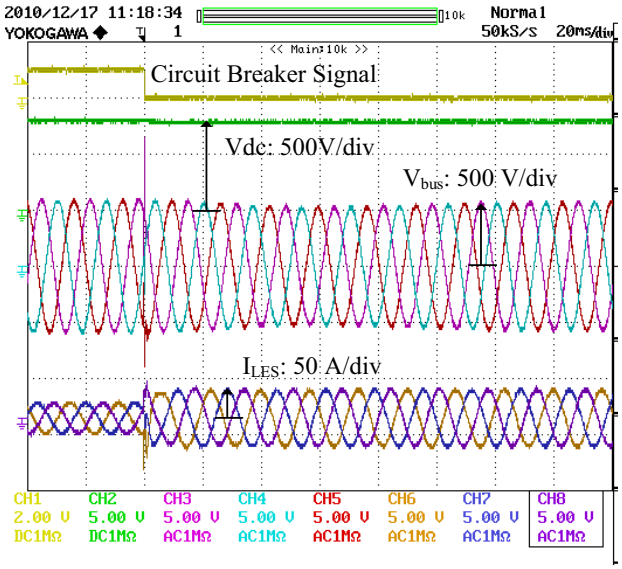

(a)

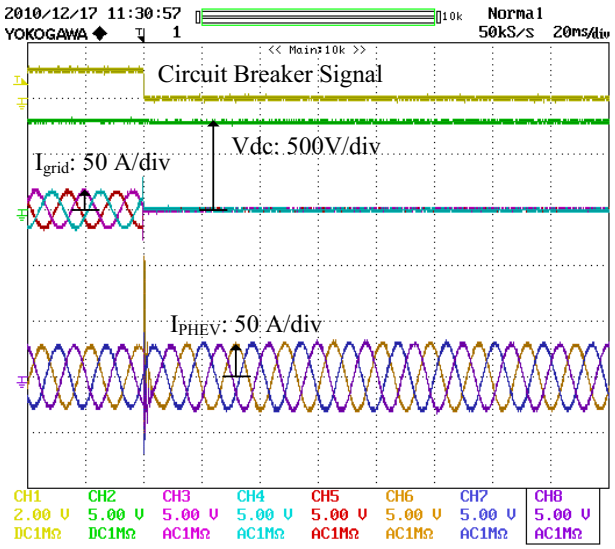

(b)

Fig. 8. Simulation Results

IV. Conclusions

This paper dealt with two important issues arising in scenarios with high-level of penetration of PHEVs and/or renewable energy sources: sizing of the local energy storage devices and the circuit level control for multiple inverter/converter systems. The effectiveness of the proposed control strategies was verified with advanced real-time simulations.

REFERENCES

[1] W. Kempton and J. Tomić, "Vehicle to Grid Fundamentals: Calculating Capacity and Net Revenue," *J. Power Sources,* vo. 144, Issue 1, 1 June 2005, Pages 268-279. doi:10.1016/j.jpowsour.2004.12.025.

[2] G. B. Shrestha and L. Goel, "A study on optimal sizing of stand-alone photovoltaic stations," *IEEE Trans. Energy Conversion*, vol. 13, no. 4, pp. 373-378, Dec. 1998.

[3] M. Migliaro, "Considerations for selecting and sizing batteries," *IEEE Trans. Industry Applications*, vol. IA-23, no.1, pp.134-143, Jan. 1987.

[4] T.-Y. Lee and N. Chen, "Optimal capacity of the battery energy storage system in a power system," *IEEE Trans. Energy Conversion,* vol. 8, no. 4, pp. 667-673, Dec. 1993.

[5] C. H. Lo and M. D. Anderson, "Economic dispatch and optimal sizing of battery energy storage systems in utility load-leveling operations," *IEEE Trans. Energy Conversion, on*, vol. 14, no. 3, pp. 824-829, Sep. 1999.

[6] K.-H. Jung, H. Kim, and D. Rho, "Determination of the installation site and optimal capacity of the battery energy storage system for load leveling," *IEEE Trans. Energy Conversion, on*, vol. 11, no. 1, pp. 162-167, Mar. 1996.

[7] "IEEE Recommended Practice for Sizing Lead-Acid Batteries for Stationary Applications," *IEEE Std 485-1997* pp.i, 1997.

[8] "IEEE Recommended Practice for Sizing Nickel-Cadmium Batteries for Stationary Applications," *IEEE Std 1115-1992* , pp.0_1, 1993.

[9] J. Stevens, J. Kratochvil, and S. Harrington, "Field investigation of the relationship between battery size and PV system performance," *Photovoltaic Specialists Conference, Conference Record of the Twenty Third IEEE* , pp.1163-1169, 10-14, May 1993

[10] D.P. Jenkins, J. Fletcher, and D. Kane, "Lifetime prediction and sizing of lead-acid batteries for microgeneration storage applications," *IET Renewable Power Generation*, vol.2, no.3, pp.191-200, Sep. 2008.

[11] W. Chee, T.C. Green, and C.A. Hernandez-Aramburo, "A stochastic simulation of battery sizing for demand shifting and uninterruptible power supply facility," in *Proc. IEEE Power Electronics Specialists Conference*, 2007, pp.2607-2613.

[12] N. Saito, T. Niimura, K. Koyanagi, and R. Yokoyama, "Trade-off analysis of autonomous microgrid sizing with PV, diesel, and battery storage," in *Proc. IEEE Power & Energy Society General Meeting*, 2009, pp.1-6.

[13] F. Blaabjerg, R. Teodorescu, M. Liserre and A.V. Timbus, "Overview of Control and Grid Synchronization for Distributed Power Generation Systems," *IEEE Trans. Industrial Electronics*, vol. 53, no. 5, pp. 1398-1409, Oct. 2006.

[14] S. Huang, L. Kong and H. Xu, "Control algorithm research on seamless transfer for distributed resource with a LCL filter," in *Third International Conference on Electric Utility Deregulation and Restructuring and Power Technologies*, 2008, pp. 2810-2814.

[15] G. Shen, D. Xu and X. Yuan, "Instantaneous voltage regulated seamless transfer control strategy for utility-interconnected fuel cell inverters with an LCL-filter," in *CES/IEEE 5th International Power Electronics and Motion Control Conference*, 2006, pp. 1-5.

[16] Q. Lei, S. Yang and Peng, F.Z., "Multi-loop control algorithms for seamless transition of grid-connected inverter," in *Proc. IEEE Applied Power Electronics Conference and Exposition*, 2010, pp. 844-848.

[17] E. Inoa and J. Wang, "A PHEV charging strategy for maximized energy saving," *IEEE Trans. Vehicular Technology*, in review.

[18] A.V. Rao, D.A. Benson, C.L. Darby, M.A. Patterson, C. Francolin, I. Sanders, and G.T. Huntington, "GPOPS: A MATLAB software for solving multiple-phase optimal control problems using the Gauss Pseudospectral Method," *ACM Trans. Mathematical Software*, vol. 37, no. 2, to appear.

[19] D. Garg, M.A. Patterson, W. Hager, A.V. Rao, D.A. Benson, and G.T. Huntington, "A unified framework for the numerical solution of optimal control problems using Pseudospectral methods," Automatica, provisionally accepted for publication, December 2009.

[20] D.A. Benson, "A Gauss Pseudospectral transcription for optimal control," Ph.D. Thesis, Dept. of Aeronautics and Astronautics, MIT, November 2004.

[21] G.T. Huntington, "Advancement and analysis of a Gauss Pseudospectral transcription for optimal control," Ph.D. Thesis, Dept. of Aeronautics and Astronautics, MIT, May 2007.

[22] E. Inoa and J. Wang, "Charging Strategy Studies for PHEV Batteries based on Power Loss Model," in SAE 2010 World Congress and Exhibition, Detroit, MI, April 2010.

[23] Kevin Morrow et al., "Plug-in Hybrid Electric Vehicle Charging Infrastructure Review," U.S. Department of Energy Vehicle Technologies Program – Advanced Vehicle Testing Activity, Final Report Battelle Energy Alliance Contract No. 58517, November 2008. Available: http://avt.inel.gov/pdf/phev/phevInfrastructureReport08.pdf

[24] R. Pena, J.C. Clare, and G.M. Asher, "Doubly fed induction generator using back-to-back PWM converters and its application to variable-speed wind-energy generation," in *Proc. IEE Electric Power Applications*, 1996, pp. 231-241.

[25] C. Gajanayake, D. Vilathgamuwa, and P. Loh, "Development of a comprehensive model and a multiloop controller for Z-source inverter DG systems," IEEE Trans. *Industrial Electronics*, vol. 54, no. 4, pp. 2352-2359, Aug. 2007.

[26] L. Qin, S. Yang, and F.Z. Peng, "High-performance and cost-effective multiple feedback control strategy for standalone operation of grid-connected inverter," in *Proc. IEEE Applied Power Electronics Conference and Exposition*, 2010, pp. 854-860.